CLAS-NOTE 93-009

AUGUST 17, 1993

GEANT Simulation of CLAS Forward Calorimeter Performance

Raphael Demirchyan

Yerevan Physics Institute

Contents

1 Introduction.

The CLAS forward region corresponding to polar angles between 5° and 45° is covered by the Electromagnetic Calorimeter (EMC) consisting of six independent and geometrically similar modules — one in every sector. Each module is a lead-scintillator sandwich made out of BC-412 plastic scintillator (10 mm thick) plates followed by lead (2.2 mm) plates.

The active volume of one EMC module represents a cut triangular pyramid with an imaginary vertex in the CLAS target point and with an active area about of 8 m^2.

Every triangular scintillator layer is sliced parallel to the one edge of this triangle into the 36 equal width strips. This slicing alternates with each edge of the triangle so that each orientation U, V or W (see **Figure 1**) repeats in every fourth plate. Altogether, there are 39 scintillator layers, consisting of three sets of 13 layers with similar strip orientation. Every scintillator strip of the same number (out of 36) from the five inner layers, nearest the target, is connected to one PMT. A similar connection is realized in the next eight outer layers having U,V or W orientations accordingly. The independent readout of inner and outer parts of the calorimeter provides for longitudinal shower sampling.

The total radiation thickness of a EMC module, including face cover plate (0.2 $X_\circ$), is about of 16 $X_\circ$.

2 Simulation.

In this note we consider some results of a Monte Carlo simulation of electromagnetic showers in the EMC induced by electrons in energy range 0.5 to 4.5 GeV. The main topics of discussion are the basic characteristics of the calorimeter such as: linearity of the energy scale, energy resolution, and uniformity of response with respect to event topology.

The simulation was performed with the software package GEANT-3.14 implemented for CLAS on VMS VAX. The GEANT simulation allows one to obtain realistic results for electromagnetic showers, limited only by the precision with which one describes the experimental setup.

In comparison with previous simulations [1] the following improvements should be noted in the present calculations, taking account:

- scintillation light attenuation
- photo-electron statistics

These corrections are both based on experimental measurements performed at the CLAS test facility for each EMC scintillator strip. Test studies show one can fit the individual strip's response A_i by an exponential

$$A_i = A_o \cdot e^{-x/l_i}$$

where x is the irradiated "point" distance (or hit coordinate) from the PMT and l_i stands for the "attenuation length". A_o depends on scintillator material qualities as well as light readout system characteristics, and test results show that it relates to the number of photoelectrons per 1 MeV, in our case by $n_{pe} = 7.5/MeV$.

In the simulation any energy deposition E_i in any scintillator is reduced by an exponential factor depending on which strip (l_i) and where (x) it occurs, then this deposition is transformed and interpreted as a measurable signal ("channel number" below or "pulse height") according Poisson statistics with a mean value $(E_i \cdot n_{pe})$.

3 Shower Profile and Leakages.

Figure 2 shows the spatial distribution of the number of secondary particles $N(X, L)$ in the shower as a function of the longitudinal coordinate (given by the active readout layer number L in EMC) and transverse coordinate X as a deviation from incident electron direction at $E_o = 4.5\ GeV$. The distribution is proportional to the energy deposition E .

Figure 3 represents the shower transverse profile — $\sum_{L=1}^{39} N(X, L)$ in linear (3_a) and logarithmic (3_b) scales for 4.5 GeV electrons. The shadowed area, including 95% showers' concentration, corresponds to $\approx 4\ cm$. Shower collimation has a very weak dependence on the incident energy, and it remains in practice constant at all energies considered .

Figure 4_a shows shower longitudinal profiles — $\int N(X, L)dX$ vs. shower depth (layer number in EMC) for different E_o and normalized to the same number of incident electrons. As in the previous figure one can find consistence in simulated shower behavior with well-known theoretical regularities.

However, closer inspection shows that all curves in fig. 4 show a step at last layer L=39. This fact is a direct indication for longitudinal shower leakage in the EMC. As is well-known [1,2,3], energy leakage in a shower calorimeter leads to linearity deviations and to degradation of energy resolution, especially at higher energies.

In present paper special attention is paid to leakages for the following reason: for a sandwich calorimeter, at the given sampling interval, there are a number of factors influencing the detector's response vs $E_\circ$ — photoelectron statistics , light attenuation, and leakages. One can easily switch "on" or "off" the former two factors in the simulation program and directly compare the influence of those factors, unlike the third one which requires a special approach.

In order to obtain a quantitative estimate of the EMC response due to the existence of leakages an additional, similar, module of the EMC was positioned in GEANT program after the ordinary one — out of six modules. This is a convenient way of having a detector thick enough to be essentially free of leakage and simple enough to have the fewest changes in program. Any statement in the following concerning layer numbers in EMC equal to $78 = 2 \cdot 39$ refers to the "doubled" calorimeter while 39 — to a common EMC module.

Shower longitudinal profiles calculated this way are shown in **Figure** 4_b in logarithmic scale. Table 1. represents leakages' percentage defined as

$$\frac{\sum_{L=40}^{78} \int E(X,L)dX}{\sum_{L=1}^{39} \int E(X,L)dX}$$

Table 1.
Percent leakages in EMC

$E_\circ$ (GeV)	Leakage (%)
0.5	0.8
1.0	1.1
1.5	1.3
2.0	1.6
3.0	1.9
4.0	2.1
4.5	2.2

4 Linearity of EMC.

The linearity of the energy scale of EMC has been studied in the incident electron energy range $E_\circ = 0.5$—$4.5\ GeV$. For any $E_\circ$ the distribution of total deposited energy E in the entire EMC is practically Gaussian with mean value E_d and dispersion $(\sigma_E)^2$ as illustrated in **Figure 5** for extremal energies. The figure shows pulse height distributions, taking account photoelectron statistics without light attenuation in scintillator strips. The same picture one can see in a denser scale in **Figure 6** for all simulated incident energies related to absolute energy depositions in 39 and 78 layers.

In **Figure 7** is shown the dependence of fitted values of centroids of those Gaussians — average energy depositions in the total EMC vs $E_\circ$.

The function $E_d = a \cdot E_\circ$ (solid line) fits the simulated dependence with $a = 0.289 \cdot GeV^{-1}$ which gives the largest deflection from linearity at energy $4.5\ GeV$ of about 0.5%. In same Figure dot line displays the linearity curve for the "doubled" calorimeter. As one can see, on account of leakages the detector has a quite different linear response but not straighten one at higher energies.

5 Uniformity.

The uniformity of the EMC response with respect to incident electron coordinate on the calorimeter surface was investigated with incident energy $E_\circ = 1\ GeV$ in the case of absence of magnetic field in the CLAS.

The response of the calorimeter was calculated at 17 points uniformly

covering the active surface of calorimeter excluding the $\approx 25\ cm$ wide zone along the triangular border of the EMC. This exclusion was chosen to avoid any boundary effects when the electron induced shower could be accepted by the calorimeter only in part. According to Figure 2 25 cm guarantees absence of shower transverse leaks.

Let's consider the detector uniformity related to different conditions in term of light attenuation in scintillator strips :

5.1 Transparent Scintillators ($l = \infty$)

Figure 8 illustrates the EMC pulse height distributions for scanned points. The histogram relates to the central point of the calorimeter ($\vartheta = 25°$, $\varphi = 0°$) and the other curves are Gaussian fits for all other points. One can make sure the mean pulse heights remain constant, however they come indistinguishable within the statistical accuracy (the relative $r.m.s$ is 0.25%).

Thus the EMC response is believed to be fully uniform for electromagnetic showers under the conditions considered.

5.2 Constant Attenuation Length ($l = 300cm$)

As a conclusion of the latter discussion one can use the technique used in [1] , where an equal energy deposition in scintillator strips running in the U,V and W orientations with constant light attenuation is assumed (i.e. consider normally incident electrons at any scanning point).

Figure 9 shows the result of such analytic calculations in the case of $l = 300\ cm$. This value is consistent with the average attenuation length in test measurements for scintillator strips belonging to the first EMC module.

One can see that the EMC pulse height deviations relative to the central point's value are less than $12 - 13\%$ unless we consider the very boundary regions where the assumption of equal energy deposition as in the center of EMC is not correct.

5.3 Measured Attenuation Lengths

The measured values of attenuation lengths for individual strips were put simulation program. As of the date of calculation only 90% of that informa-

tion was available and missing information (mostly with higher layer numbers : ≥ 30) was generated according to the measured distributions.

The EMC module was mapped in a way described in beginning of this Section.

The resulting scatter plot shown in **Figure 10** should be considered as one for the first module EMC of CLAS. Response deviations are still within the limits as in 5.2 which allows one make use of the EMC electron energy information in the data aquisition trigger. The observed small asymmetry caused by local differences between scanned points in terms of attenuation.

6 Energy Resolution.

6.1 Contributions to Resolution

The energy resolution for normally incident electrons in the middle of the calorimeter was investigated in detail. The simulation performance allows one to extract information concerning the relative contribution of each component of the final compound energy resolution; namely 1) fluctuations due to EMC sampling; 2) photoelectron statistics ; 3) energy leakages and 4) light attenuation.

Simulation results are summarized in **Figure 11** which displays the normalized energy resolution $\sigma_\circ \equiv \sqrt{E_\circ(GeV)}\sigma_E/E$ dependence on $E_\circ$ in the case of transparent scintillators (left fig.) and for constant attenuation $l = 300\ cm$ (right fig.). In both figures, boldface symbols relate to the "doubled" EMC in the absence of leakages and light symbols relate to the ordinary EMC module.

Sampling fluctuations one can evaluate having $\sigma_\circ(E_\circ)$ dependence for "doubled" EMC when not only leaks but also all other fluctuations mentioned above have been switched off and thus only shower intrinsic fluctuations are considered for the given calorimeter sampling. This component in $\sigma_\circ$ turns out to be σ_{sp}=6.8%.

Leakage fluctuations cause a different behaviour of $\sigma_\circ(E_\circ)$ concerning the "doubled" calorimeter compared with a common one in similar conditions ($l = \infty$ or $300cm$). The available statistical accuracy (1000-2000 generated events) gives a range for σ_{lk} equal to $(1.6 - 1.9)\sqrt{E_\circ}$ percent.

It should be stressed that there is no direct relation between Table 1 data

and this evaluation: in the first case (Table) we have integral characteristics of leakages, when the σ_o expresses the scale of their fluctuations.

Photoelectron statistics is a source of uncertainties in energy resolution included in the simulation in a known form from the beginning (see Section 2) originating from the chosen photoelectron number $n_{pe} = 7.5/MeV$.

a) In the case of *transparent* scintillators, when no reduction on n_{pe} occurs, we have $\sigma_{ph} = 2.14\%$.

b) Due to light *attenuation* in the scintillator strips σ_{ph} increases by the factor α of this attenuation. Because all strips are supposed to have the same coefficient $l = 300\ cm$ and for all energies E_o we consider the same incident direction for electrons ($\vartheta = 25°$, $\varphi = 0°$), α is constant and calculations show $\alpha = 1.56$ which gives eventually $\sigma_{ph} = 3.34\%$.

Both of these values for σ_{ph} are completely consistent with subtraction results of corresponding data shown in Figure 11.

Light attenuation and transmission uncertainties revealed in two ways: any scintillation light attenuation, as well as transmission inefficiency, leads to the

a) reduction of measurable signal and as a consequence degradation of photoelectron statistics

b) and put his own dispersion concerning nonlinearity of transformation of initial distribution in one hand, and second, nonuniformity both in strips attenuation characteristics ($l \neq const$) and fiber readout system inefficiency ($\eta_f \neq const$).

This makes one believe — to get more realistic evaluation for σ_o we need information in terms of $l, \eta_f \neq const.$ concerning scintillator strips involved in shower registration.

Let's note in advance, in simulation program $\eta_f = 1.0$ is assumed because of absence of needed test results so far. However, in case of $\eta_f \neq const$, one can make corrections on the light transmission from scintillator strips to the fiber readout optics, eventually, to the calorimeter pulse height. This correction may considerably reduce the fluctuations of the measured signal from EMC, as one can find in discussion below.

In order to get more realistic information about energy resolution presented in Figure 11 one can use results of EMC mapping from section 5 with measured attenuation lengths l. The analysis shows, besides the pulse height deviations equal to 12% over the mapped area EMC, the absolute variation of the normalized resolution is in limit $\leq 1\%$ at $E_o = 1GeV$. This excess is

close to $\sigma_o(4.5GeV)$; $l = 300\ cm$ and it's expected to have resolution close to the projected $\leq 10\%$ at $4.5GeV$.

The EMC was not completely mapped at 4.5 GeV. However , a worse case, a point was investigated near the corner, with relatively bad scenery of attenuations of the scintillator strips which gives $\sigma_o(4.5\ GeV) = 9.1\%$. The upper curve in **Figure 12** represents an interpolation between resolutions 1 and 4.5 GeV for the $CLAS$ first sector EMC module. In the same way we simulated the second module of the EMC which has measured $l_{average} \approx 400\ cm$ i.e. with a higher average value than in sector one (also with higher spread). This curve is shown the second from top in figure 12.

These two curves show very close estimations for σ_o concerning EMC modules for the $CLAS$ first and second sectors accordingly, although the latter one has slightly systematic better resolution.

For comparison , in figure 12, the curves related to the "ideal" case ($l = \infty$) and the scenario with $l = 300\ cm$ are shown also.

6.2 Correction for Attenuation Lengths

For any shower there are six different groups of scintillators composing the entire thickness of EMC — 39 layers, namely — three readout views (U, V, W) with two sampling parts i.e. inner and outer.

In order to compensate for the spread of the average attenuation lengths between these groups, a correction procedure was accomplished. For any primary electron a $P = 3\ GeV/c$ muons passing was simulated through the same main pixels of EMC . There were found six weight coefficients w_{ij}, representing the ratios of the mean pulse heights P_{ij} in each group at $l = \infty$ to the real situation with $l \neq const$:

$$w_{ij} \equiv \frac{< P^{\mu}_{ij}(l = \infty) >}{< P^{\mu}_{ij}(l \neq const) >}$$

where the indices run

$$i = U, V, W$$
$$j = inner, outer$$

The correction was performed in the form of a substitution

$$P_{ij} \Rightarrow w_{ij} \cdot P_{ij}$$

which allows the corrected pulse heights to be treaded as in case for $P_{ij}(l = \infty)$. The resolution dependence is shown in figure 12 labelled as "corrected" both for sector one and two modules of the EMC . The resolution is still close for different modules but one can see an essential improvement over the whole curve. It could be hoped, after this correction procedure, which one may make with cosmic rays, that the normalized resolution for first two modules EMC will not excess 8.5% up to $E_o = 4.5\ GeV$.

A similar correcting procedure could be accomplished concerning the readout system nonuniformity — with coefficients η_f.

7 Acknowlegments.

We consider this work as a small step toward understanding the calorimeter response in realistic circumstances, and see a lot of room for improvement. This work has been accomplished within the context of several helpful conversations with fellow collaborators community Hall B.

We are grateful to Volker Burkert for active discussions, help and support during this work.

We acknowledge the interest and suggestions of Bernhard Mecking.

We are grateful to Will Brooks for his careful help, for long discussions and for his willingness in helping to creating this manuscript.

We would like to thank Elton Smith for proofreading portions of this manuscript.

The author would appreciate any comments concerning this work. Please send them to **DEMIRCHYAN@CEBAF.GOV**.

References

[1] V.Burkert, in CEBAF Conceptual Design Report, April 13, 1990.

[2] C.W.Fabjan and T.Ludlam, Ann. Rev. Nucl. Part. Sci., 32 (1982) 335.

[3] W.Hofmann et al.,Nuclear Instruments and Methods, 195 (1982) 474.

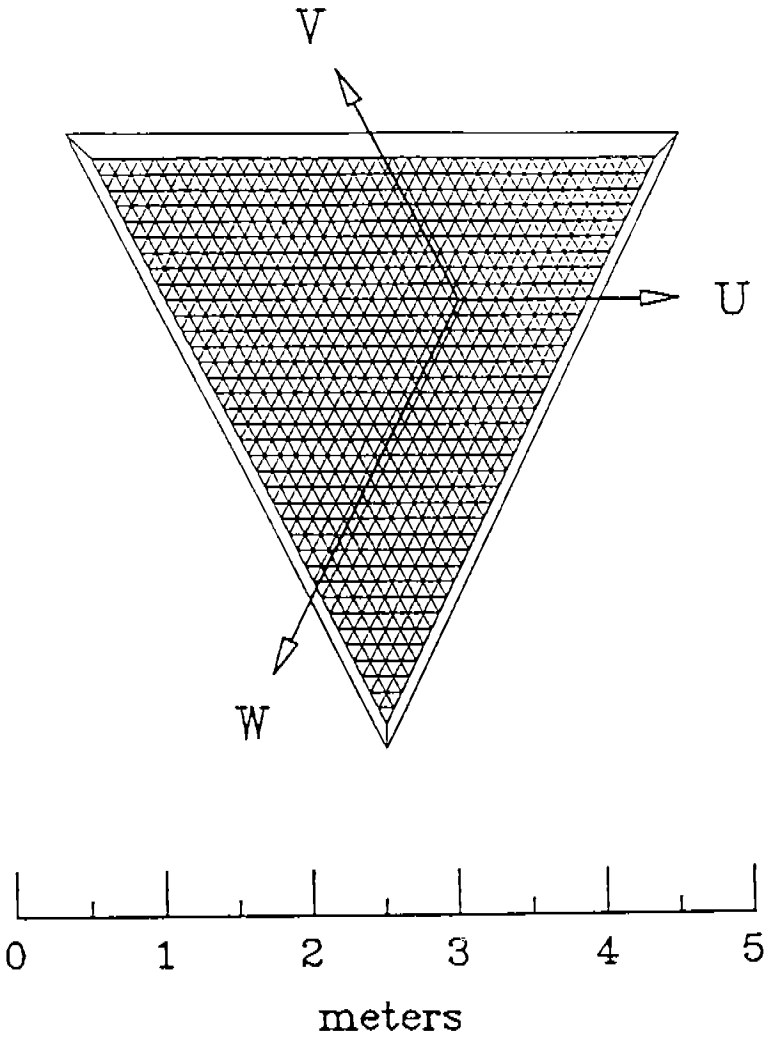

Figure 1. The active volume of a module of the CLAS forward EMC. View from target. Strip slicings are shown for the first three layers only. Scintillator read out ends are indicated by arrows.

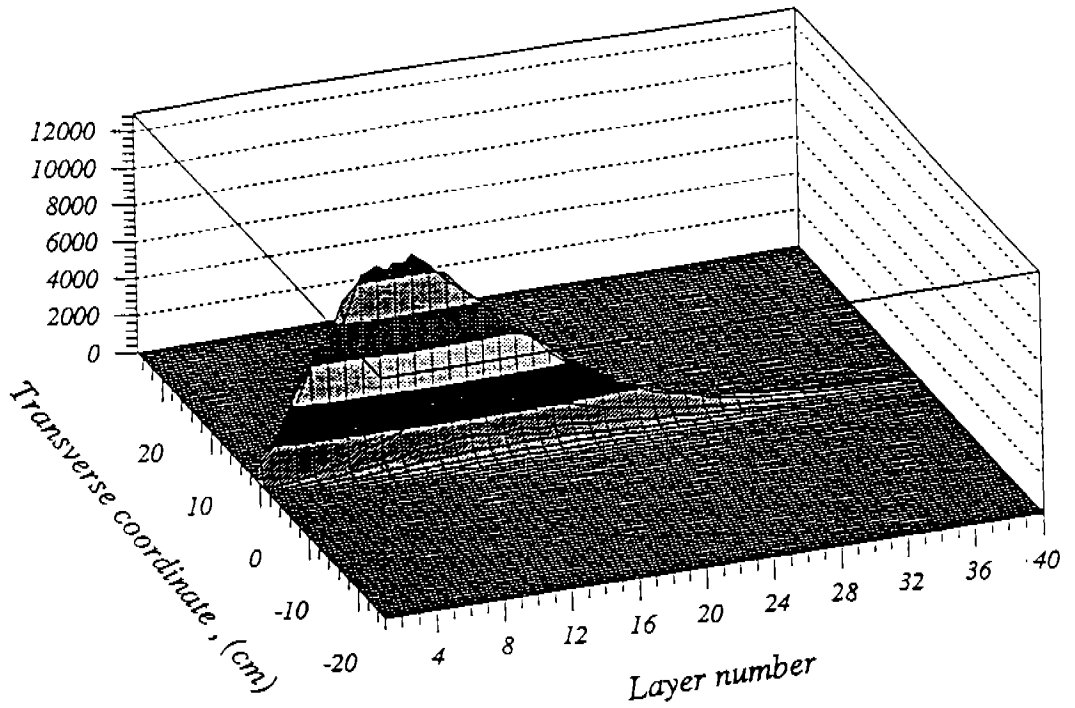

Figure 2. The spatial distribution of shower secondary particles vs. layer number in EMC and transverse deflection from the incident $E_\circ = 4.5\ GeV$ electron direction.

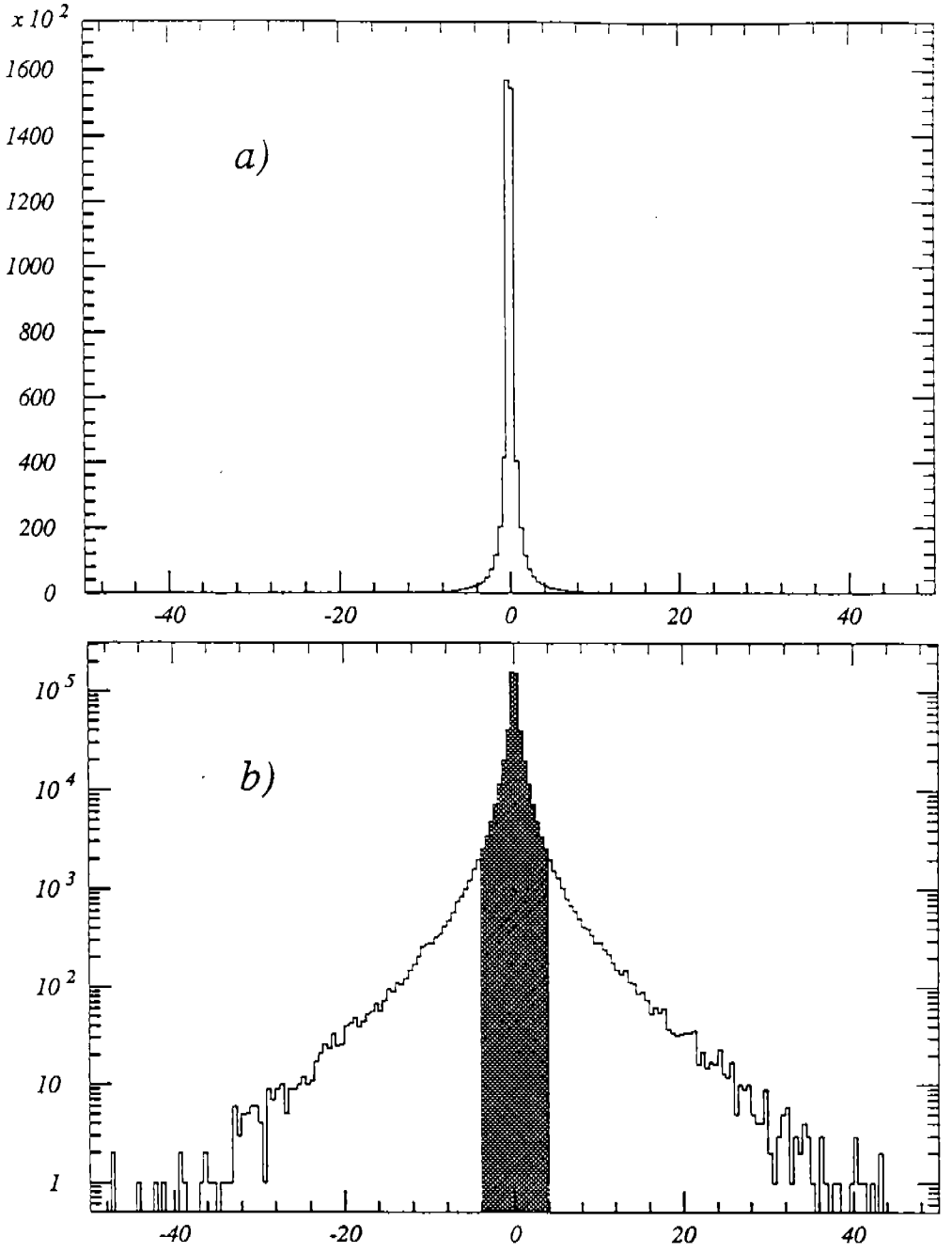

Figure 3. Simulated shower transverse profile induced by $E_\circ = 4.5\ GeV$ electrons in EMC in linear (fig. a)) and logarithmic (fig. b)) scales. Shadowed area $\pm 4\ cm$ corresponds to 95% shower collimation.

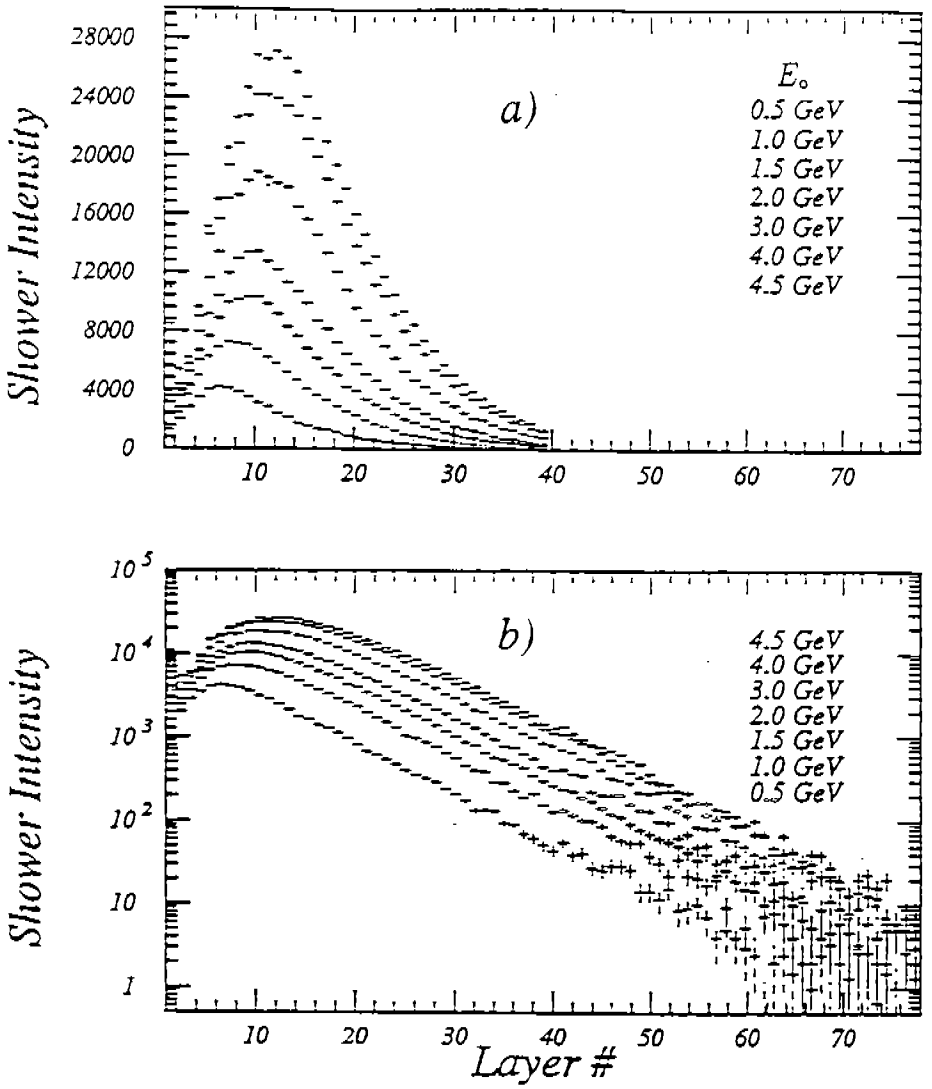

figure 4.

a) — Shower longitudinal profiles vs. shower depth in EMC for different incident energies and normalized to the one incident electron in arbitrary units.

b) — The same for calorimeter with doubled thickness.

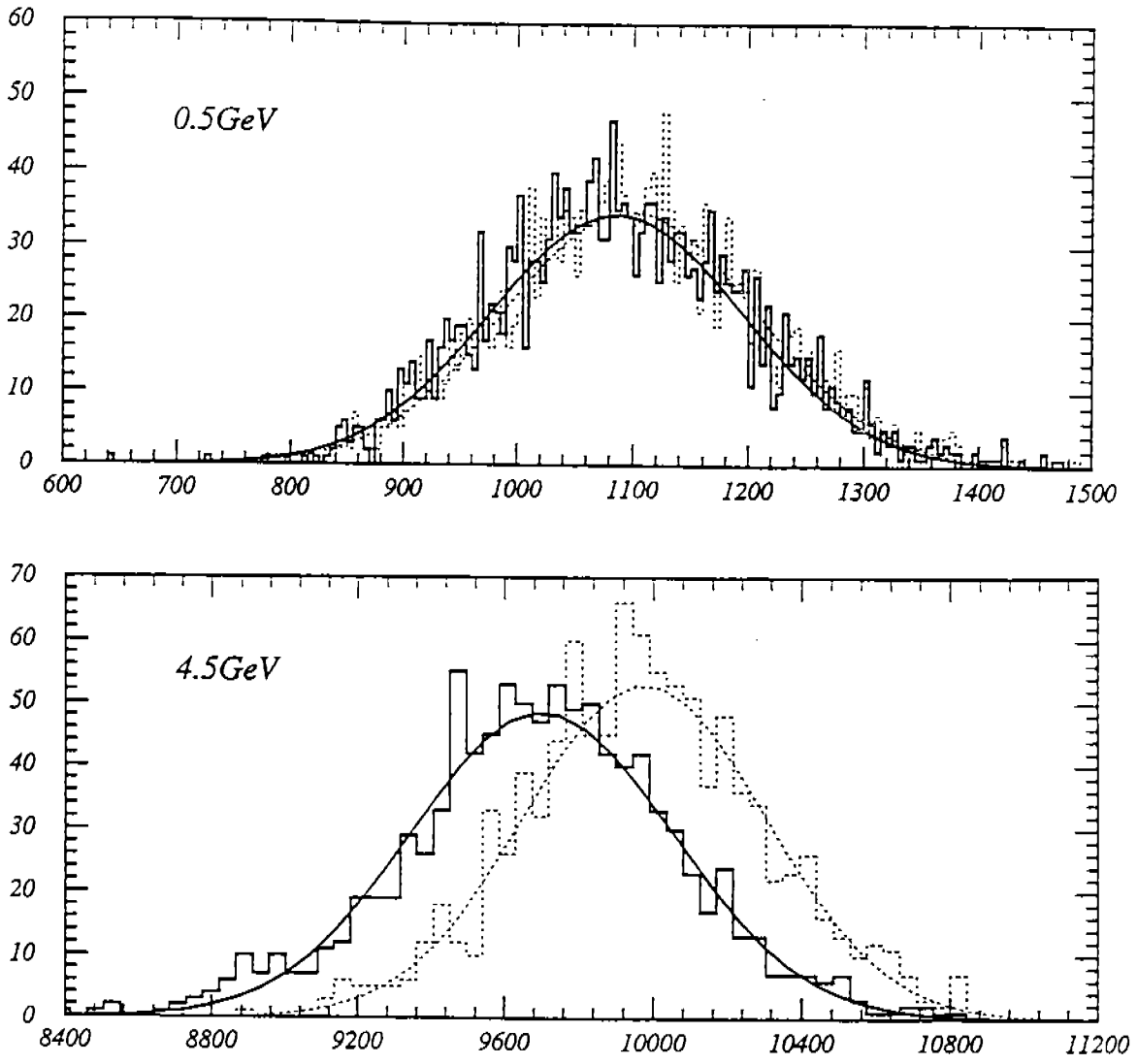

figure 5. The simulated distributions of total deposited energy in entire EMC in terms of photoelectron number for $E_\circ = 0.5\ GeV$ (upper figure) and 4.5 GeV (bottom). Curves are Gaussian fits.

Distributions related to the doubled calorimeter are shown with dots.

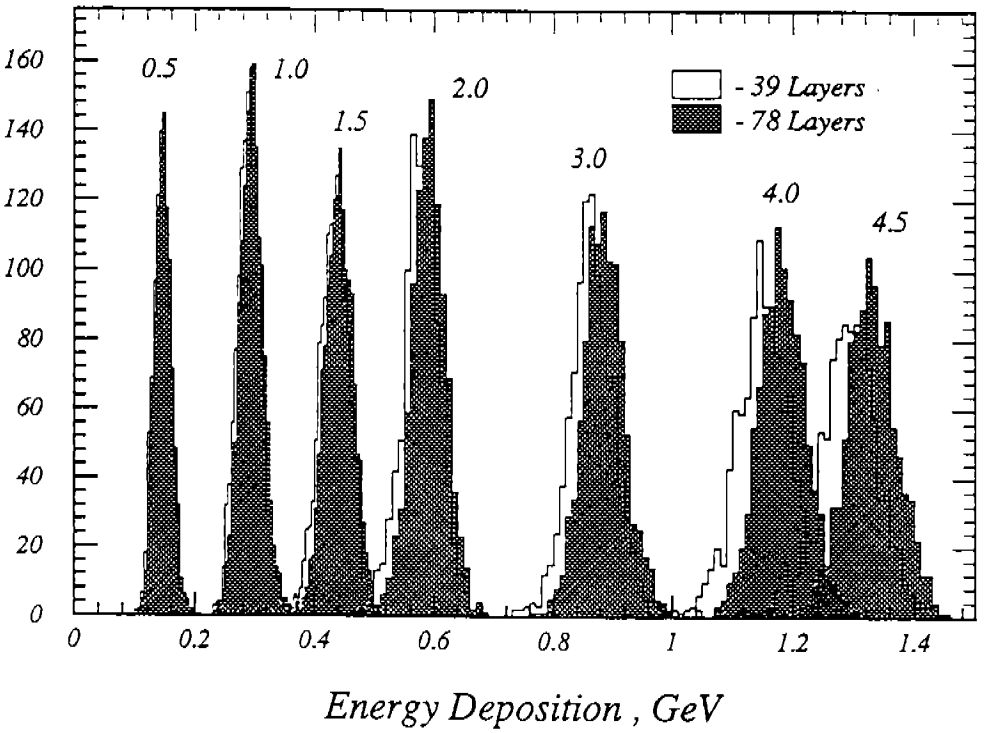

figure 6. Energy deposited in 39-layers EMC (light histograms) and 78-layers (darks) for incident energy of electrons in GeV indicated on the top of curves.

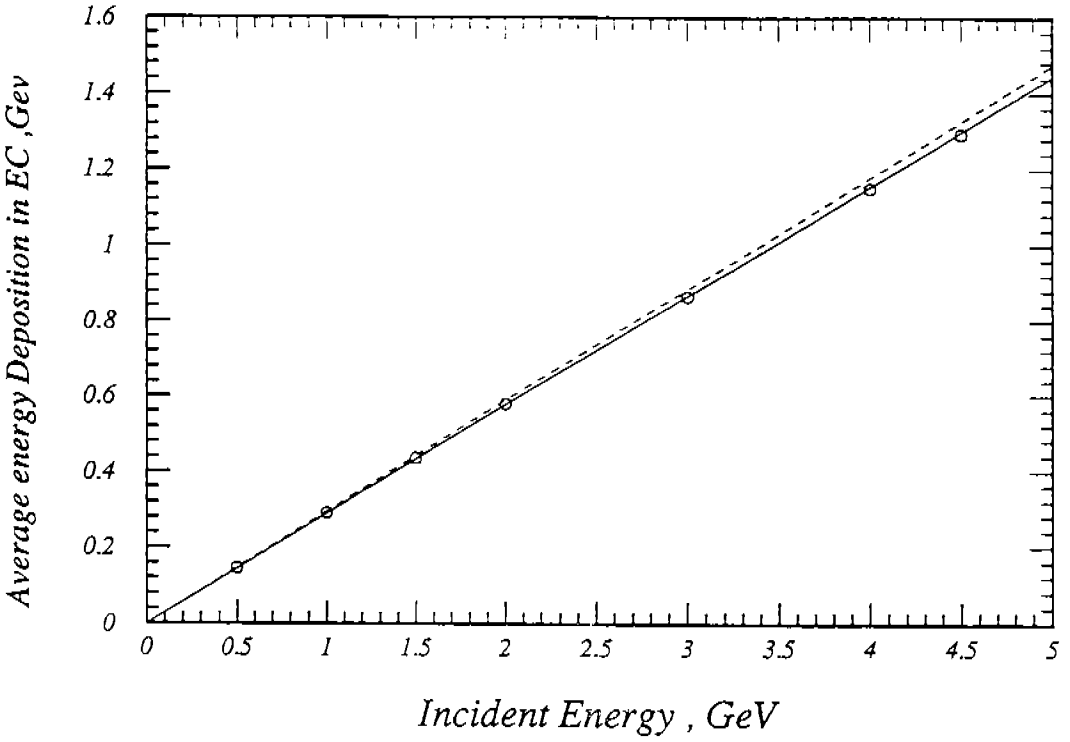

figure 7. The linearity curve of the EMC. Symbols correspond to Gaussian centroids from the previous figure. The dash line represents the linearity curve related to energy depositions from 78 layers.

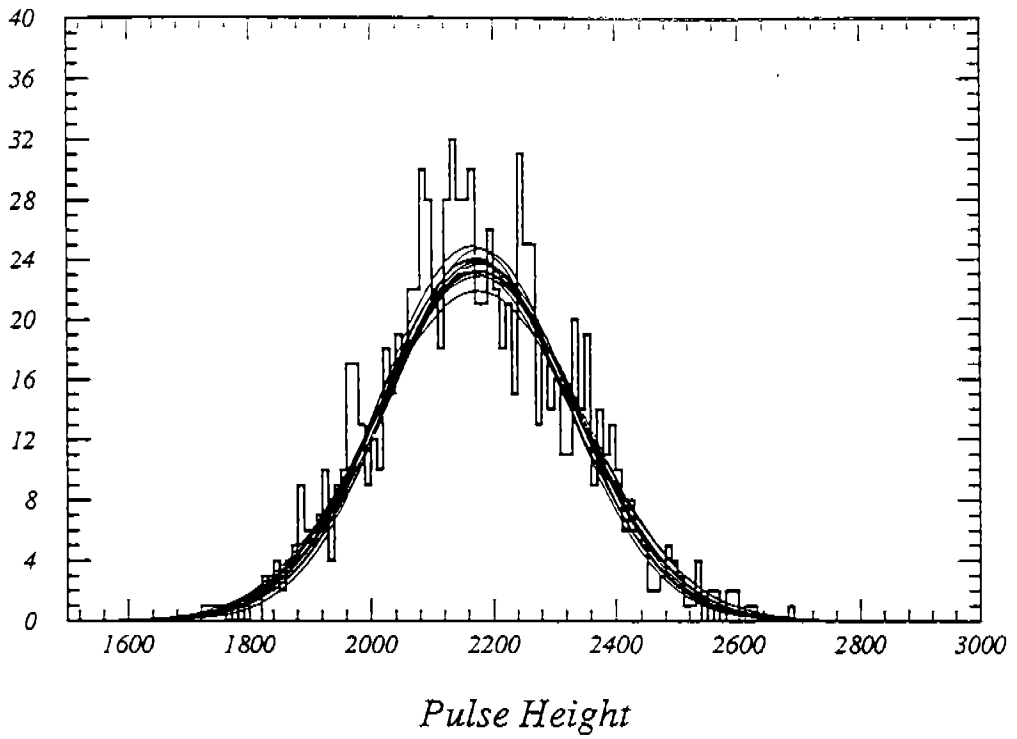

Figure 8. EMC pulse height distributions concerning 17 different incident trajectories of $E_o = 1GeV$ electrons. The histogram relates to the central point of EMC ($\vartheta = 25°, \varphi = 0°$ for the first module). Curves represent Gaussian fits for all other trajectories, having angular distance up to 29° from central one.

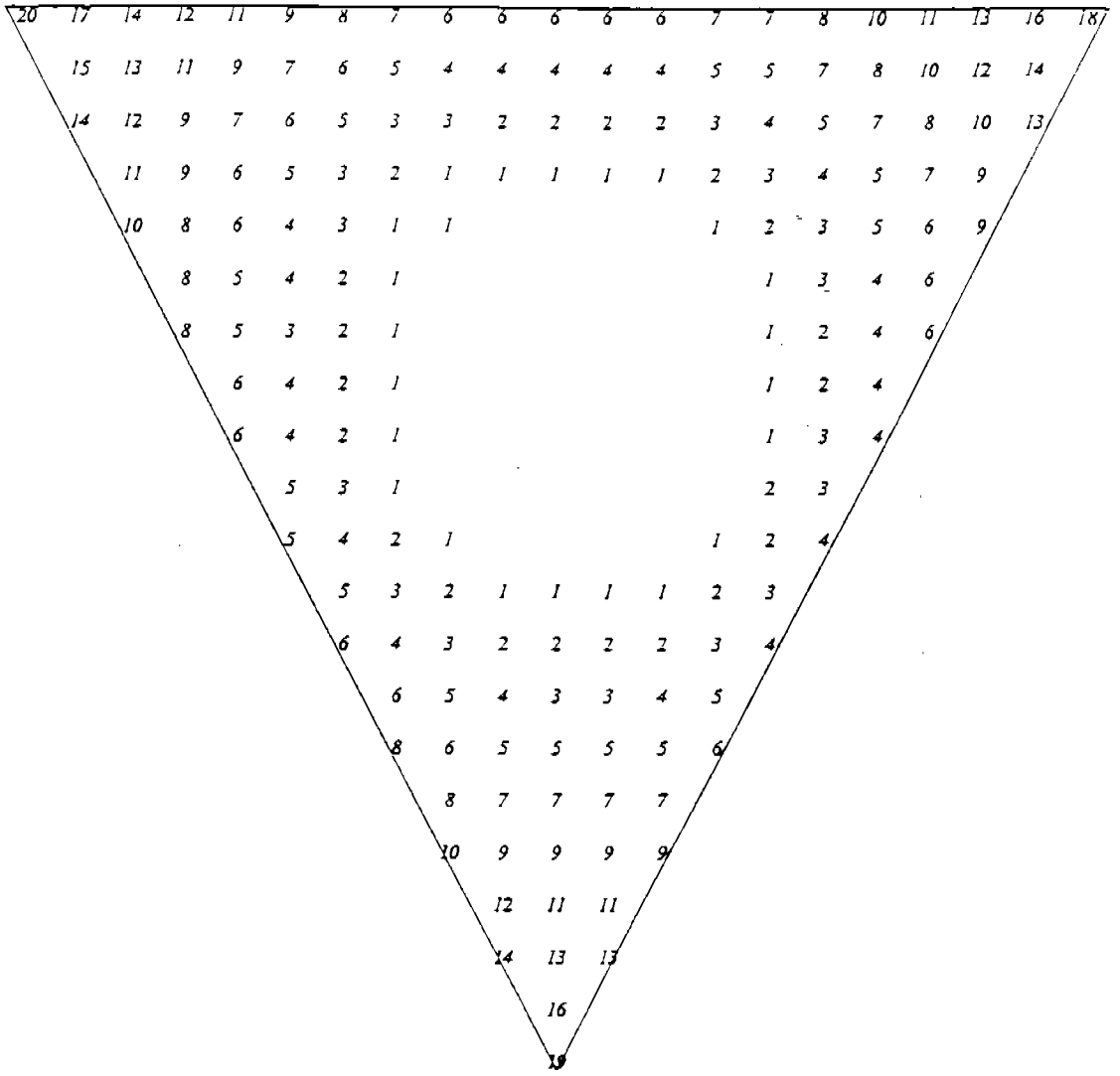

Figure 9. Deviations in percent of the EMC pulse height relative to the central point. Constant attenuation length $l = 300$ cm is assumed for all scintillator strips and equal energy depositions in all points.

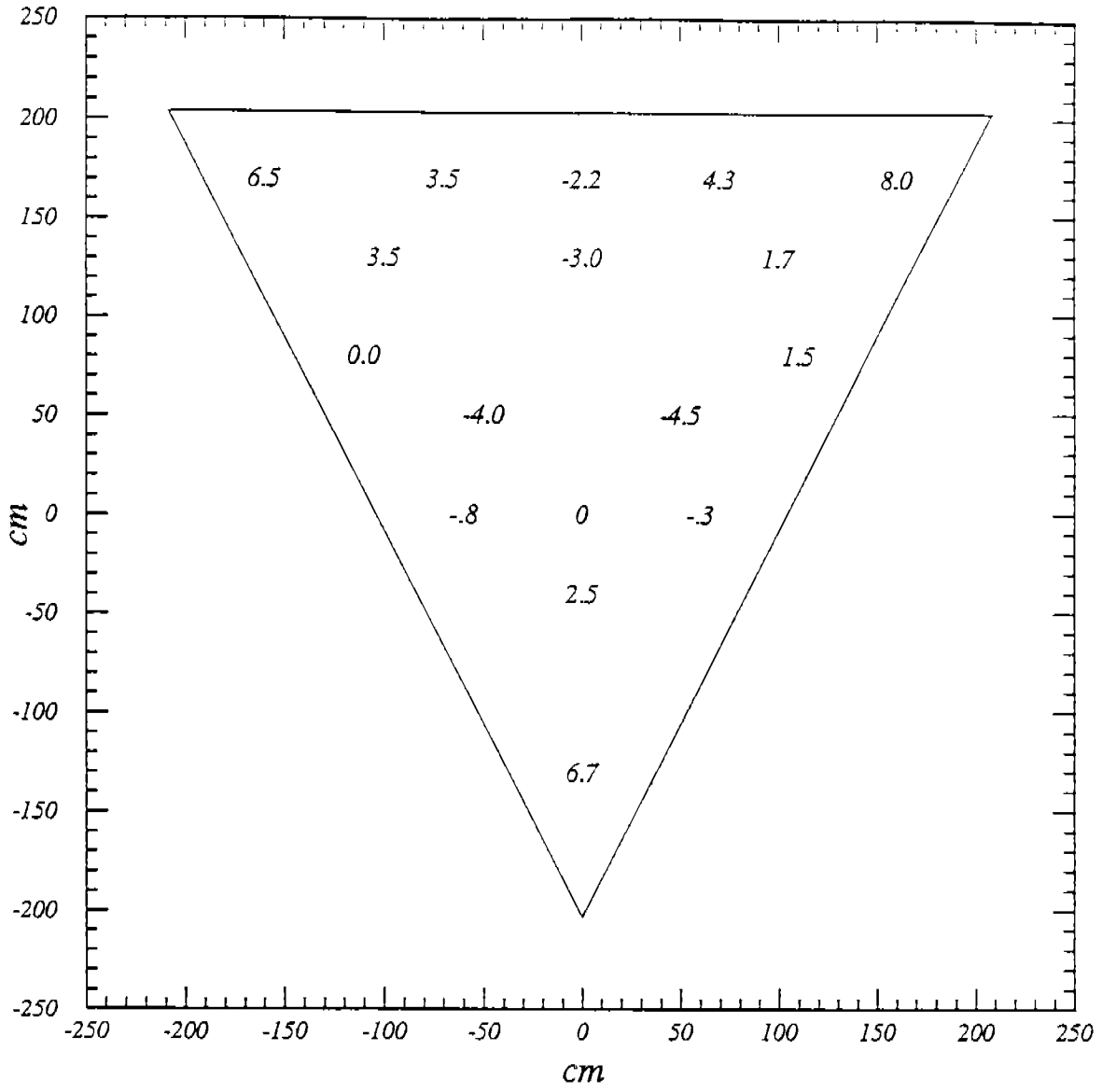

Figure 10. GEANT simulation of deviations in percent of the EMC pulse height relative to the central point. The measured values of attenuation lengths for scintillator strips were put concerning first module $EMC\ CLAS$.

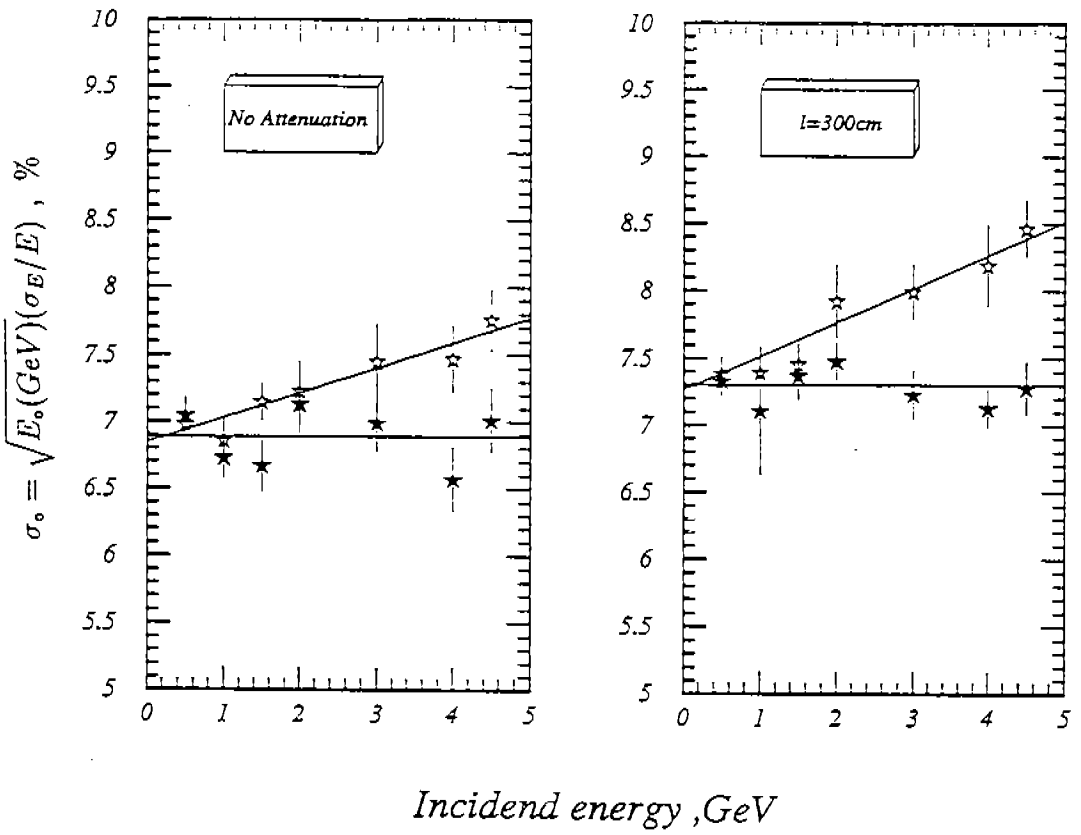

Figure 11. The normalized energy resolution dependence on incident energy. Left figure concerns transparent scintillator strips ($l = \infty$) and right one corresponds to equal attenuations in strips with $l = 300$ cm.

Dark symbols show the resolution of doubled calorimeter.

Light symbols relate to a single EMC module.

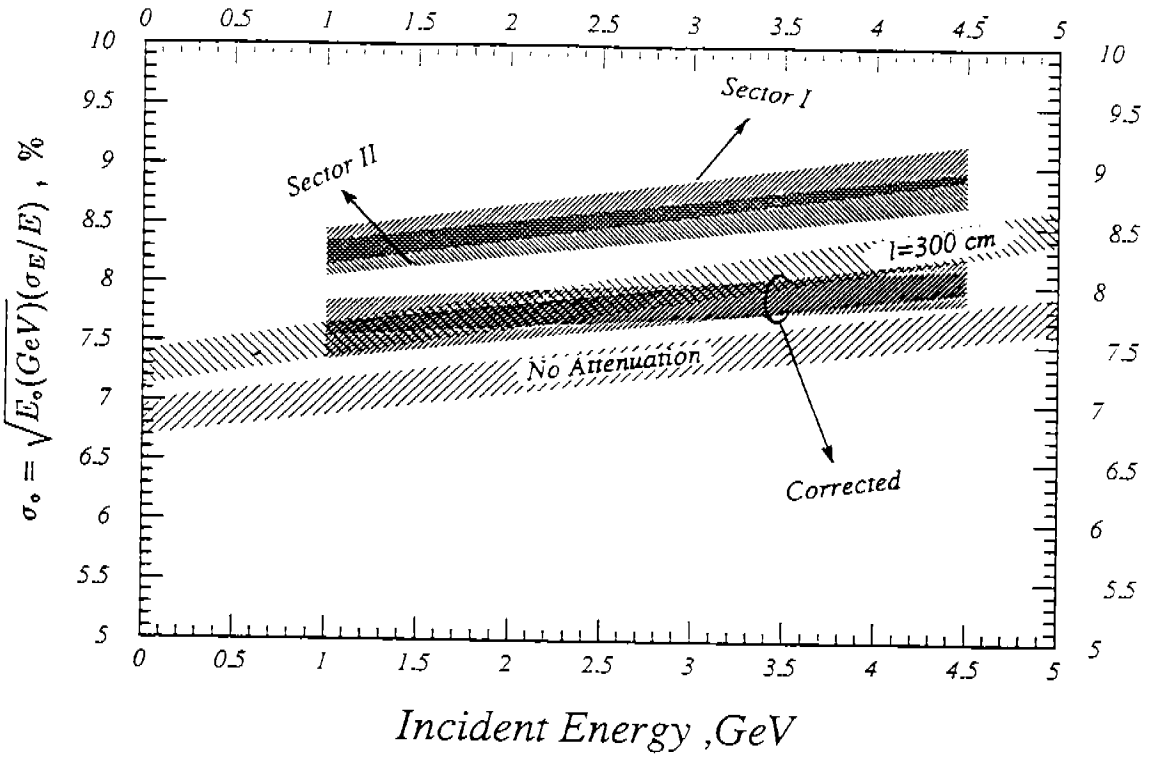

Figure 12. The normalized energy resolution dependence on incident electron energy. The curves from the previous figure are represented, corresponding to $l = 300$ *cm* and $l = \infty$.

The dependences for sectors 1&2 of *CLAS* are added with measured attenuation lengths, as well as with muon correction procedure.

The curves' '*widths*' reflect the statistical accuracy of the simulation.